

Mechanical Influence of Tissue Scaffolding Design with Different Geometries using Finite Element Study

Journal:	<i>Part H: Journal of Engineering in Medicine</i>
Manuscript ID	JOEIM-22-0435.R2
Manuscript Type:	Original article
Date Submitted by the Author:	25-Jun-2023
Complete List of Authors:	An, Xinyi ; Teesside University Chong, Perk; Teesside University, School of Science and Engineering Zohourkari, Iman ; Birjand University of Technology Roy, Dr. Sandipan; SRM University, Mechanical Engineering Merdji, Ali; University of Mascara Gnanasagaran, Constance ; Kingston University Faraji, Foad ; Teesside University Moey, Lip Kean ; SEGi University Yazdi, Mohammad Hossein ; Islamic Azad University
Keywords:	Mechanical Influence, Tissue Scaffolding, Different Geometries, Pore distribution, FEA
Abstract:	The mechanical properties of tissue scaffolds are essential in providing stability for tissue repair and growth. Thus, the ability of scaffolds to withstand specific loads is crucial for scaffold design. Most research on scaffold pores focuses on grids with pore size and gradient structure, and many research models are based on scaffolding with vertically arranged holes. However, little attention is paid to the influence of the distribution of holes on the mechanical properties of the scaffold. To address this gap, this research investigates the effect of pore distribution on the mechanical properties of tissue scaffolds. The study involves four types of scaffold designs with regular and staggered pore arrangements and porosity ranging from 30% to 80%. Finite element analysis (FEA) was used to compare the mechanical properties of different scaffold designs, with von-Mises stress distribution maps generated for each scaffold. The results show that scaffolds with regular vertical holes exhibit a more uniform stress distribution and better mechanical performance than those with irregular holes. In contrast, the scaffold with a staggered arrangement of holes had a higher probability of stress concentration. The study emphasized the importance of balancing porosity and strength in scaffold design.

Mechanical Influence of Tissue Scaffolding Design with Different Geometries using Finite Element Study

Xinyi An¹, Perk Lin Chong¹, Iman Zohourkari², Sandipan Roy^{3*}, Ali Merdji⁴,
Constance Linda Gnanasagaran⁵, Foad Faraji¹, Lip Kean Moey⁶
Mohammad Hossein Yazdi⁷

¹School of Computing, Engineering and Digital Technologies, Teesside University,
Middlesbrough TS1 3BX, United Kingdom.

²Department of Mechanical Engineering, Birjand University of Technology, Birjand,
Iran.

³Department of Mechanical Engineering, SRM Institute of Science and Technology,
Kattankulathur, Chennai 603203, India.

⁴Faculty of Science and Technology, Department of Mechanical Engineering,
University of Mascara, Algeria.

⁵Department of Mechanical Engineering, Kingston University, Roehampton Vale
Campus, London, SW15 3DW, United Kingdom

⁶Center for Modelling and Simulation, Faculty of Engineering, Built Environment &
Information Technology, SEGi, 47810, Selangor, Malaysia.

⁷New Materials Technology and Processing Research Center, Department of
Mechanical Engineering, Neyshabur Branch, Islamic Azad University, Neyshabur,
Iran.

*Corresponding Author Email: sandipan888roy@gmail.com

Abstract

The mechanical properties of tissue scaffolds are essential in providing stability for tissue repair and growth. Thus, the ability of scaffolds to withstand specific loads is crucial for scaffold design. Most research on scaffold pores focuses on grids with pore size and gradient structure, and many research models are based on scaffolding with vertically arranged holes. However, little attention is paid to the influence of the distribution of holes on the mechanical properties of the scaffold. To address this gap, this research investigates the effect of pore distribution on the mechanical properties of tissue scaffolds. The study involves four types of scaffold designs with regular and staggered pore arrangements and porosity ranging from 30% to 80%. Finite element analysis (FEA) was used to compare the mechanical properties of different scaffold designs, with von-Mises stress distribution maps generated for each scaffold. The results show that scaffolds with regular vertical holes exhibit a more uniform stress distribution and better mechanical performance than those with irregular holes. In

1
2
3
4 contrast, the scaffold with a staggered arrangement of holes had a higher probability of
5 stress concentration. The study emphasized the importance of balancing porosity and
6 strength in scaffold design.
7
8
9

10 **Keywords:** Mechanical Influence, Tissue Scaffolding, Different Geometries, Pore
11 distribution, FEA
12

13 14 **1. Introduction**

15
16 Bone remodelling is an essential process for human growth and development and the
17 bone damage is a cause of bone remodelling. However, if the lost or damaged bone area
18 is large, the bone cannot heal through its remodeling process [1]. In the repair of tissues
19 or organs, tissue transplantation and allogeneic tissue replacement have certain
20 limitations. The emergence of tissue engineering (TE) has solved this problem. Tissue
21 scaffolding provides not only mechanical functions for damaged parts but also
22 accelerates tissue repair by incorporating biological factors that can be used to stimulate
23 tissue repair to the scaffold [2]. Bone tissue engineering scaffolds also have individual
24 requirements as a substitute for modern biological bone. Excellent scaffolding should
25 strike a balance between biocompatibility and mechanical properties [3]. Scaffolding
26 needs to be biocompatible, biodegradable, and will not produce harmful substances to
27 disrupt the environmental balance in the body. While being highly porous, the
28 mechanical properties of its structure should also be excellent, with a certain degree of
29 toughness and load-bearing capacity, providing a particular automated environment for
30 tissue repair [4].
31
32
33
34
35
36
37
38
39
40
41
42
43
44
45
46
47

48 Metals have been studied as materials for tissue scaffolding due to their promising
49 mechanical properties and biocompatibility. These materials exhibit physical properties,
50 such as Young's modulus, that closely resemble those of bones, but surpass bones in
51 terms of structural strength and stability [5]. Among them, Titanium, as one of the
52 biocompatible elements, is a promising material for implants and compared to solid
53 ones, porous structures offer several advantages. As an example, implants with porous
54 materials show improved bone ingrowth [6-7]. The range of Young's modulus of human
55
56
57
58
59
60

1
2
3
4 bone tissue is about 4-30 GPa [8]. Due to the risk of stress shielding, it is crucial to
5 ensure that the Young's modulus of the scaffold matches that of the surrounding tissues.
6 Titanium alloy is an optimal choice as it has a lower Young's modulus than traditional
7 alloys, allowing for a closer match to the natural bone structure. Additionally, this
8 material offers excellent corrosion resistance, making it an attractive option for medical
9 applications [9]. A porous titanium scaffold shows a good match with bone tissue. It
10 can promote the growth and differentiation of cells on the scaffold [10], and by
11 adjusting the porosity in the structure of a titanium scaffold, it can have more suitable
12 mechanical properties for implantation in the human body [11].
13
14
15
16
17
18
19
20
21
22

23 The emergence of computer-aided tissue engineering (CATE) has become an
24 indispensable field in tissue engineering [12]. Among various analysis methods, finite
25 element analysis (FEA) is an effective method in modelling mechanical responses of a
26 scaffold structure. Most studies have shown that the mechanical performance results
27 simulated by FEA are basically consistent with the actual compression test results [13-
28 14], which significantly reduce the cost of experiments for evaluating performance of
29 custom scaffolds [15]. Numerical simulations are mainly used to obtain the apparent
30 Young's modulus and to check the strength of tissue scaffolds. These two mechanical
31 properties are related to whether the scaffold can have a certain support ability in the
32 body or not [16]. To prevent stress shielding [17], whether tissue engineering
33 scaffolding can simulate the mechanical properties of human bone is a crucial concern
34 [18]. Titanium alloy as the material and modelled as Schwarz's minimal surface based
35 on the ISM method. The finite element results show that the stiffness of the scaffold
36 model obtained by parameterization meets the stiffness range of human cortical bone
37 [19]. As a functionally graded structure of bone, its mechanical strength will change
38 with the arrangement. The emergence of functionally graded scaffolding (FGS) is to
39 simulate the changing structure of natural bones designed a three-layer gradient lattice
40 based on FGS to achieve functional gradient by changing the thickness of the support
41 rod [20-21]. Compared with a uniform crystal lattice, the design of a graded crystal
42 lattice can meet the different requirements for mechanical properties of different parts.
43
44
45
46
47
48
49
50
51
52
53
54
55
56
57
58
59
60

1
2
3
4 Different from network structure, it has proved that a gradual lattice scaffold based on
5 the sheet structure has better absorption capacity and stable growth of absorption
6 efficiency and moreover, shows a better mechanical property [22]. In addition, to satisfy
7 the mechanical properties similar to those of natural bone, the biocompatibility of the
8 scaffold must also be satisfied. The proliferation and growth of osteoblasts as an
9 example to study the biological activity of functionally graded titanium alloy structures.
10 The results show that this structure is conducive to cell adhesion and proliferation [23].
11 In vitro cell tests conducted on scaffolds that meet the range of mechanical properties
12 of human bones. They also used Ti6Al4V as the material to design three scaffolds that
13 change the strut orientations to change the structure. In vitro tests show that human
14 osteoblasts have a strong ability to synthesize on this titanium scaffold [24]. Compared
15 to untreated scaffolds with mechanical properties similar to human cancellous bone, the
16 biological activity of porous titanium scaffolds that have undergone chemical treatment
17 and heat treatment has been significantly improved [25].

18 For the design of the pores of tissue scaffolds, most of the scaffolds as mentioned above
19 consider the design factors of the scaffold pore size or gradient pores, and the
20 arrangement of the holes is usually orderly. The purpose of this research is to explore
21 the influence of pore distribution on the mechanical properties of scaffolding. Four
22 design types of scaffolds were considered. Finite element analysis (FEA) was used to
23 compare the apparent Young's modulus of different design types with regularly
24 arranged pores and staggered pores. Besides, to predict the influence of porosity on
25 various design parameters, the scaffold porosity range of 30% to 80% were studied.

2. Methodology

2.1 Design Porous Scaffolding

26 The Siemens NX software is used to produce 3D models of scaffolds. Through the
27 standard Boolean process, the pore structure is superimposed on the cube and the
28 cylinder. The superimposed pore structure is circular and square, thus eight different
29 designs of scaffolds were created as shown in Figure 1. Changing the shape of the basic
30

unit block of the scaffold and its porosity and hole arrangement are the main design methods. The cubic scaffold is in $10\text{ mm} \times 10\text{ mm} \times 10\text{ mm}$, where the cylindrical scaffold is in 10 mm diameter and 10 mm height. Cylindrical structures A and B display regular square and circular porous arrangements measuring $0.98\text{ mm} \times 0.98\text{ mm}$ and 1.1 mm in diameter, respectively, while structures A' and B' exhibit the same patterns but in a staggered arrangement. Cubic structures C and D also show regular square and circular porous arrangements of the same dimensions, with staggered arrangements present in structures C' and D'.

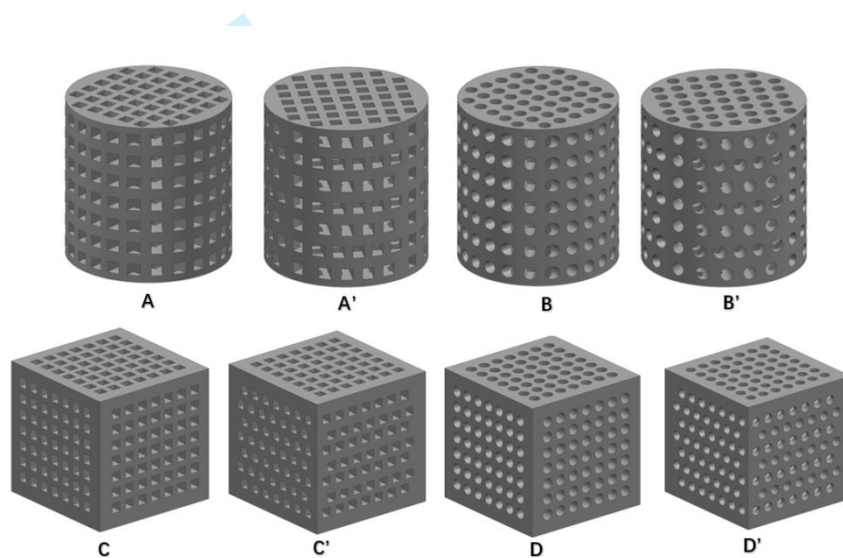


Figure 1: Porous Scaffolds (A) Cylindrical with regular square porous arrangement (A') Cylindrical with staggered square porous arrangement (B) Cylindrical with regular circular porous arrangement (B') Cylindrical with staggered circular porous arrangement (C) Cubic with regular square porous arrangement (C') Cubic with staggered square porous arrangement (D) Cubic with regular circular porous arrangement (D') Cubic with staggered circular porous arrangement

The apparent Young's modulus of natural bones decreases with porosity increasing. To satisfy mechanical properties and biological activity, the porosity is usually set in the range of 66% to 88% [26]. In this study, the porosity used was 30 to 80% to investigate the influence of the pore distribution on the mechanical properties of the scaffold and explore the range of porosity in which the titanium scaffold meets the range of apparent Young's modulus of human bone.

1
2
3
4
5
6 The porosity is the percentage of the pore volume to the original total volume of the
7 material without openings. Know the volume of the designed unit porous model through
8 the software. The porosity of the designed tissue engineering scaffold is defined
9 according to the following formula
10
11

$$P = \left(1 - \frac{V_{Rem}}{V}\right) \times 100\% \quad (1)$$

12
13
14
15
16
17
18 Where V_{Rem} is the volume of the cell porous model and V is the original volume of the
19 model.
20

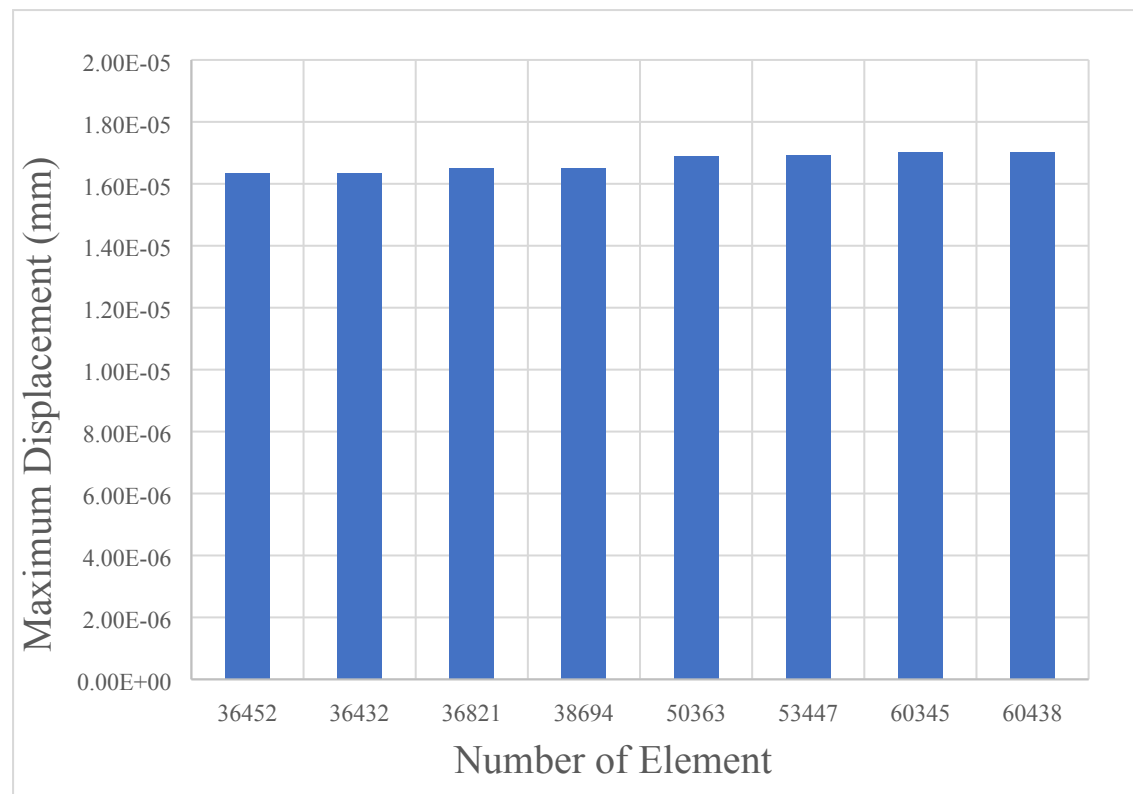
21
22
23
24 The number of holes for each designed scaffold and the position of the holes on the
25 scaffold are the same. The porosity here is mainly obtained by controlling the size of
26 the holes. By keeping Constant the pore size and changing numbers and their
27 distribution, different porosities can be obtained. However, to obtain a scaffold with a
28 specific porosity, due to the change in porosity, the distribution and number of pores
29 on the scaffold will also change, which may result in very different internal structures
30 with different porosities. The internal structure may also affect the mechanical
31 properties of the scaffold. Therefore, to avoid this situation, the size of the pores has
32 been changed to obtain different porosities.
33
34
35
36
37
38
39
40
41

42 **2.2 Finite element analysis (FEA)**

43
44 Siemens NX12 was used for the finite element models to predict the mechanical
45 responses of different designs of tissue scaffolds and evaluate the influence of porosity
46 on the apparent Young's modulus of scaffolds. The material used for numerical analysis
47 is titanium alloy (Ti6Al4V) which is an excellent bone substitute material. Its material
48 properties are assigned as Young's modulus $E=110$ GPa and Poisson's ratio $\nu=0.3$.
49

50
51 To balance the accuracy of the FE model and the calculation time, the sensitivity of the
52 mesh was analyzed, Figure 2 shows the Convergence graph of a cubic scaffold with a
53 50% porosity square hole. Considering the geometric intricacies, the use of a hexagonal
54 mesh may lead to distorted meshes. Thus, for accurately capturing the significant
55
56
57
58
59
60

1
2
3
4 variations in porosity, it is more practical to use a 3D tetrahedron elements despite the
5 overall simplicity of the geometry. Additionally, to ensure the reliability of the obtained
6 results, a mesh convergence study has been conducted as shown in Figure 2. Based on
7 the convergence study the grid size of 0.7mm is selected and respective number of
8 elements is 60345 as shown in Figure 3.
9
10
11
12
13
14
15
16
17
18
19
20
21
22
23
24
25
26
27
28
29
30
31
32
33
34
35
36
37
38
39
40
41
42



43 Figure 2: Convergence of Maximum Displacement with Respect to Number of
44 Element
45
46
47
48
49
50
51
52
53
54
55
56
57
58
59
60

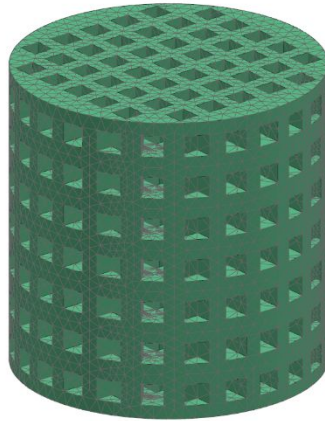


Figure 3: 3D Model with 0.7mm mesh size

The boundary conditions used to evaluate the mechanical performance of the scaffold are shown in the Figure 4. A simulated axial compression test was carried out on the model. A force was applied to face block A in axial direction, and constraints were added to the opposite face of the scaffold to prevent its displacement. The total axial force applied to the shown surface is equal to 5N.

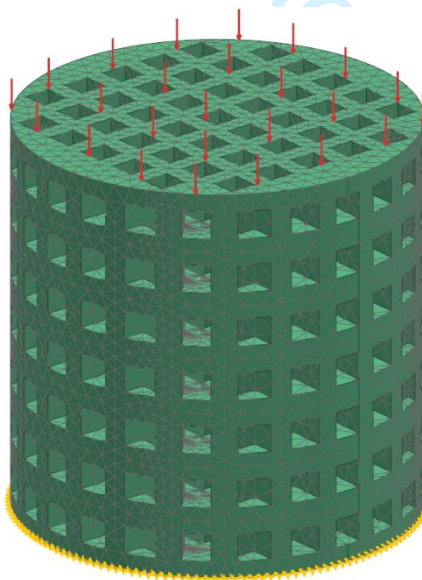


Figure 4: Boundary condition and load applied to the scaffold

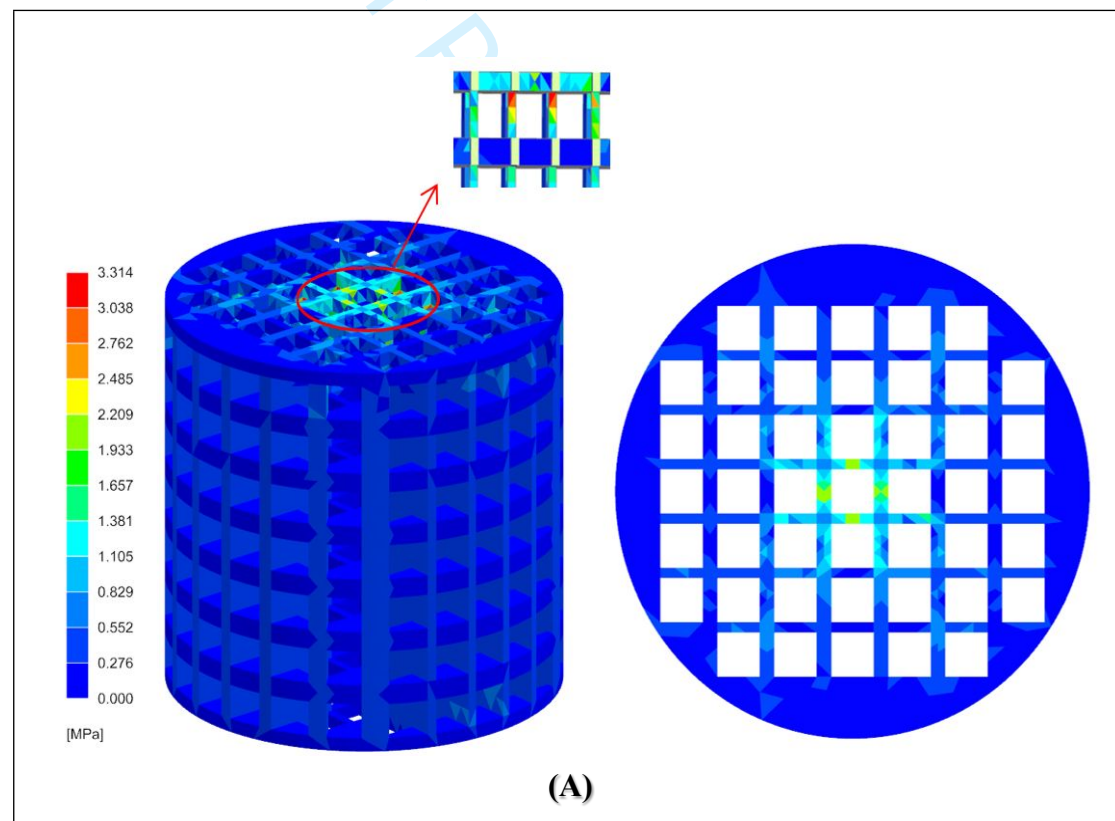
Considering the load amount and displacement results obtained by FEA simulation, the apparent Young's modulus of scaffolds with different porosities were calculated by

applying formula (2). Since the apparent Young's modulus of the scaffold under a specified porosity is constant, it can be seen from the formula that the magnitude of the applied load will not affect the apparent Young's modulus of the scaffold, so for easy calculation, the force applied here is 5N.

$$E_S = \frac{FL}{A\Delta L} \quad (2)$$

Where F is the applied load, L is the initial length of the model, A is the initial cross-sectional area, and ΔL is the displacement of the support after the load is applied.

3. Results and discussion



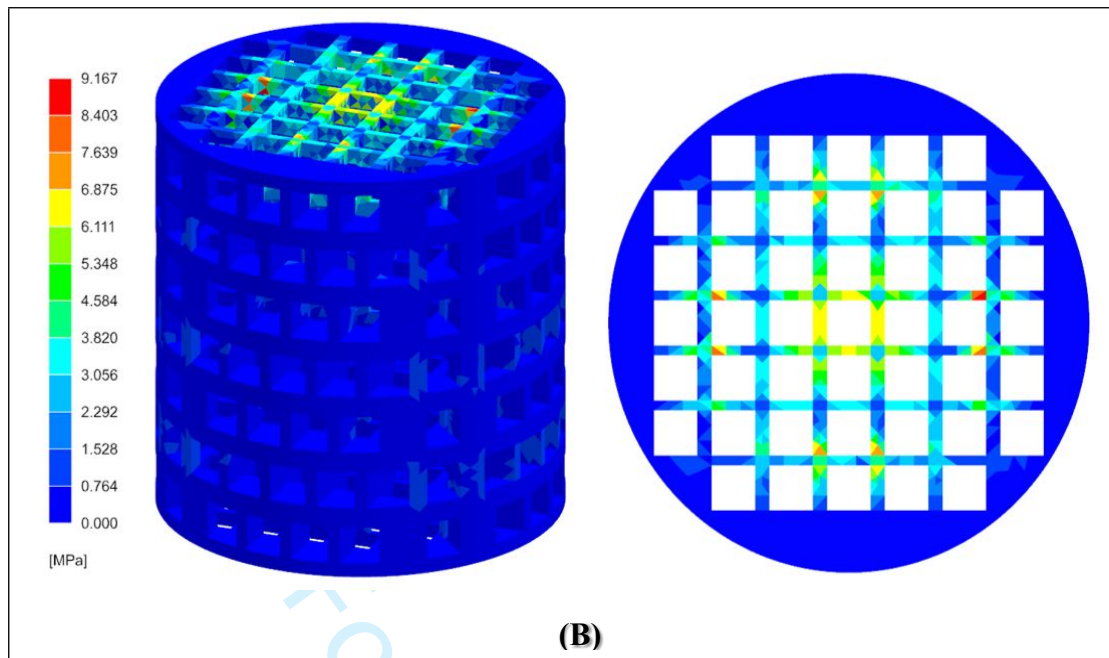
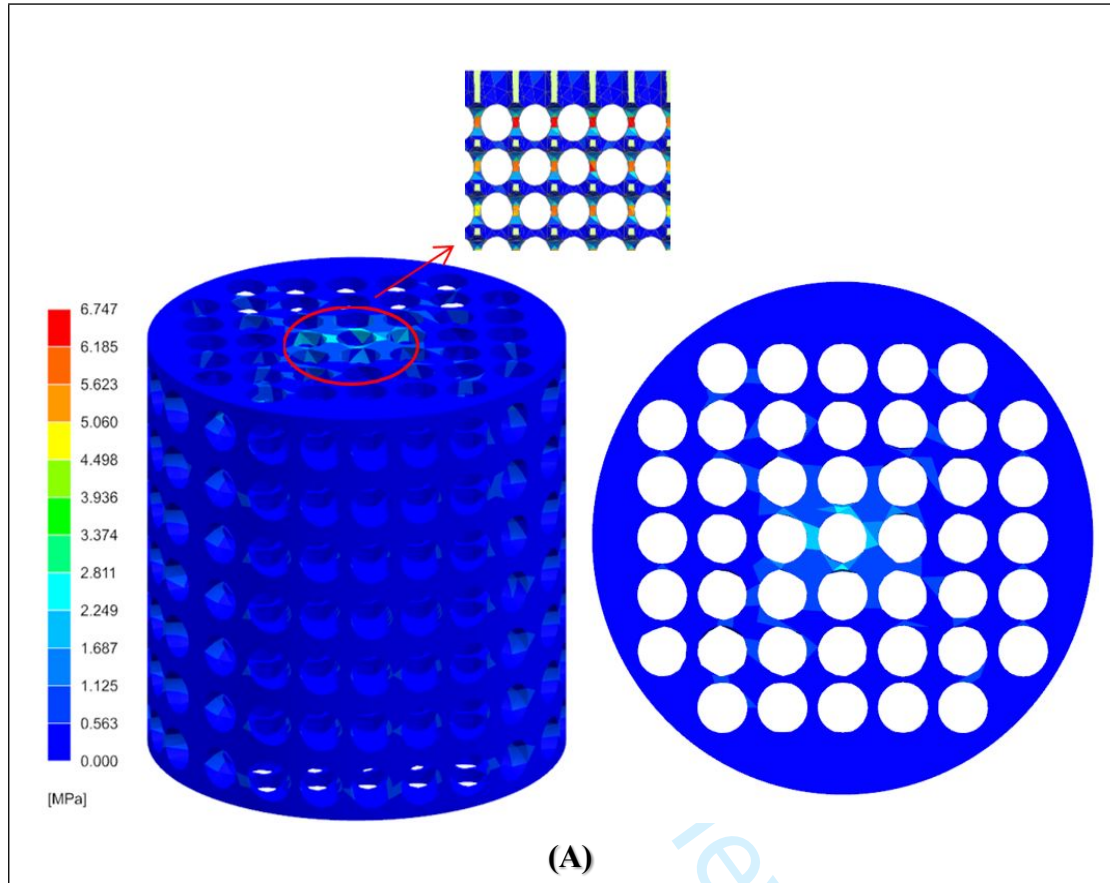


Figure 5: von Mises stress distribution of cylindrical scaffold with square hole.

Finite element models for eight types of scaffolds with regular and irregular holes were developed and their mechanical properties were calculated. Figure 5 shows the von Mises stress distribution of a scaffold with a cylindrical basic unit shape. For tissue engineering scaffolds, it is generally believed that scaffolds with high porosity can better promote cell aggregation and blood vessel formation. However, too high porosity will reduce the mechanical strength of the scaffold [27]. Therefore, it is very important to make a balance between porosity and strength of a scaffold. So, von Mises stress distribution map of the scaffold with a porosity of 70% is selected here.

As shown in Figure 5 (A), the maximum stress of a scaffold with vertically ordered holes mainly occurs at the pillar below the loading surface. The maximum stress of the scaffold with staggered holes in Figure 5 (B) is concentrated on the round surface. The stress of the scaffolds of both designs can be seen on the surface where the load is applied. Compared with the regularly arranged square-hole scaffold (Figure 5A), the stress of the staggered-hole scaffold B is more widely distributed on the circular surface, and the maximum stress is on the loading surface. In a recent study, similar stress

1
2
3
4 distribution was obtained where the stress was highest on loading surface [28]. Its stress
5 concentration distribution is regular, symmetrical up and down, and mainly distributed
6 on the pillars far from the center of the cross section. The maximum stress of A is
7 smaller than that of B, which is about one-third.



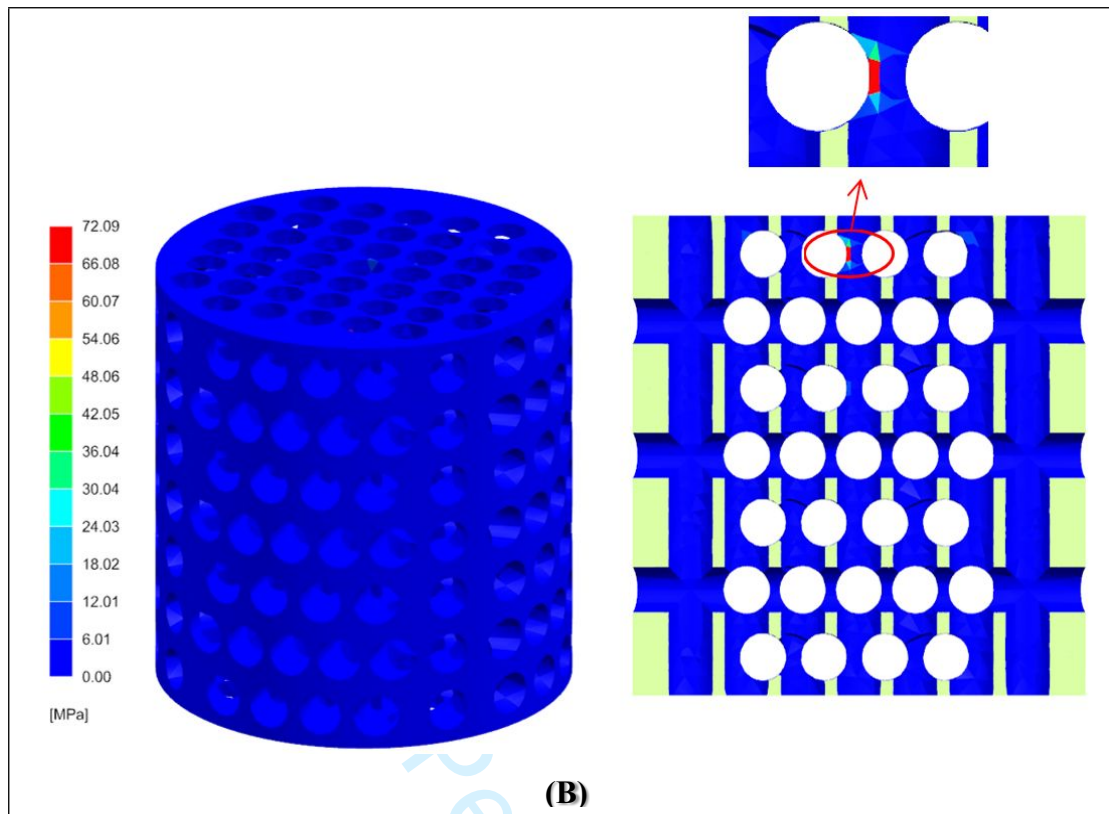


Figure 6: von Mises stress distribution of cylindrical scaffold with round hole

As for the stress distribution of the scaffold with round hole type, as shown in Figure 6, different behaviours are observed, and their stress is almost not distributed on the round surface. The stresses in Figure 6 (A) and (B) are mainly concentrated on the central pillar inside the scaffold and closest to the loading surface. The farther away from the centre of the loading surface, the smaller the stress of the A scaffold. The stress concentration of the staggered round-hole scaffold (B) is mainly concentrated on the pillars near the centre of the circle. And its maximum stress value is the largest among all scaffolds designed, as high as 72.09 MPa, which is about 11 times that of regularly arranged scaffolds. In all cylindrical scaffolding, the maximum stress of a scaffold with regular vertical holes is smaller than that of a scaffold with irregular holes. Among the four models, the lowest maximum stress Figure 5(A) is 3.314 MPa.

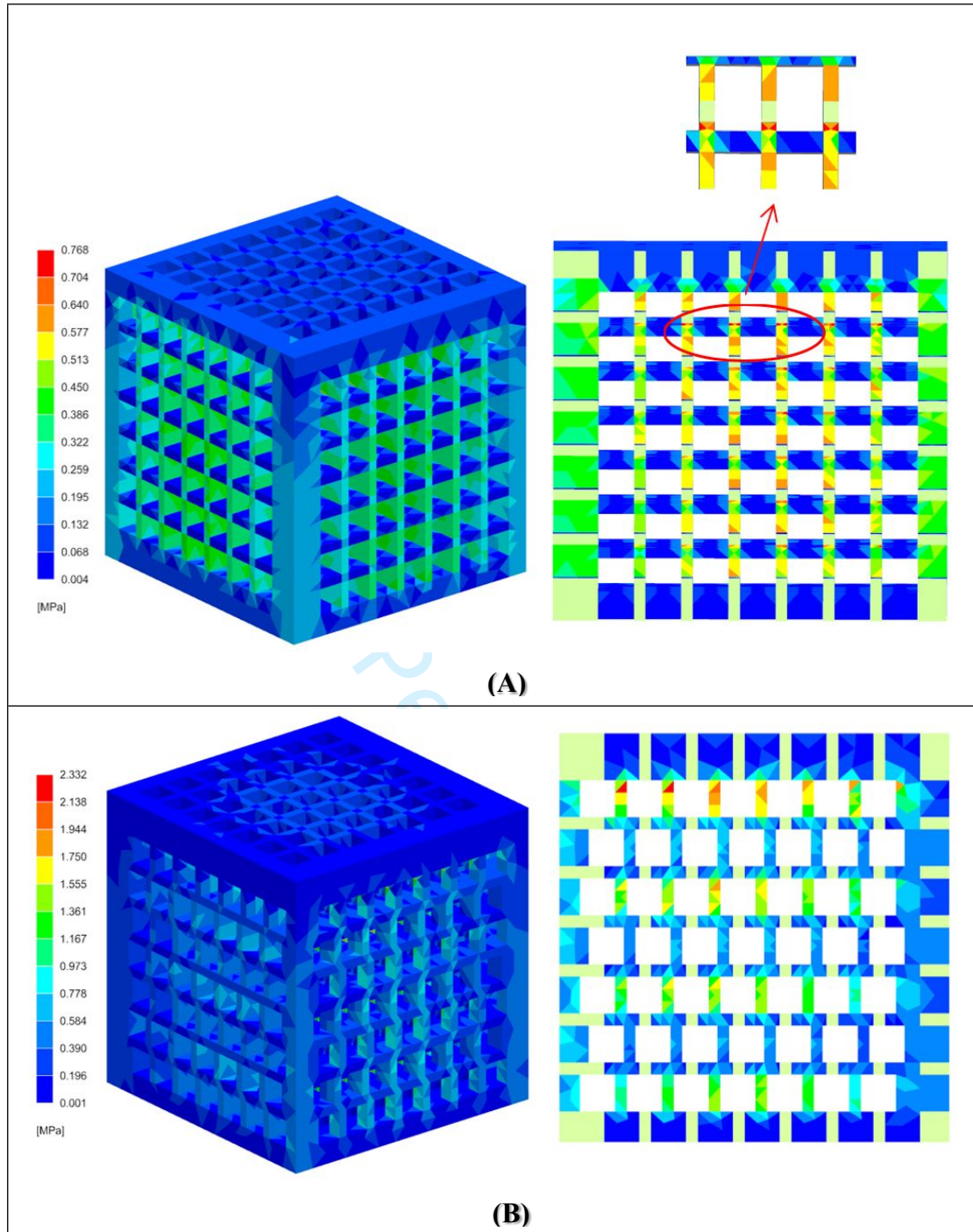


Figure 7: von Mises stress distribution of cubic scaffolding with square hole

Different from the porous cylindrical element scaffold, the von Mises stress distribution of the cubic element scaffold is mainly located inside the scaffold. Figure 7 (A) shows that the scaffold with square holes arranged vertically shows a more uniform stress distribution. The stress of scaffold A is mainly concentrated on the pillars in the same direction as the loading load. The stress on the vertical pillar is minimal and almost 0.

1
2
3
4 Similar results were obtained for cubical shape scaffold design. In the experimentally
5 validated FEM, showed that the stress distribution has same pattern as the study [29].
6
7 In another study, similar results were obtained the stress was high on the porous area
8 of their proposed cubical shape scaffold, while no stress occurs on the diagonals [30].
9
10 Its loading capacity is better, and the maximum stress is only 0.768 MPa. The stress
11 distribution of the scaffold with irregularly arranged holes (Figure 7(B)) is concentrated,
12
13
14
15
16
17
18
19
20
21
22
23
24
25
26
27
28
29
30
31
32
33
34
35
36
37
38
39
40
41
42
43
44
45
46
47
48
49
50
51
52
53
54
55
56
57
58
59
60

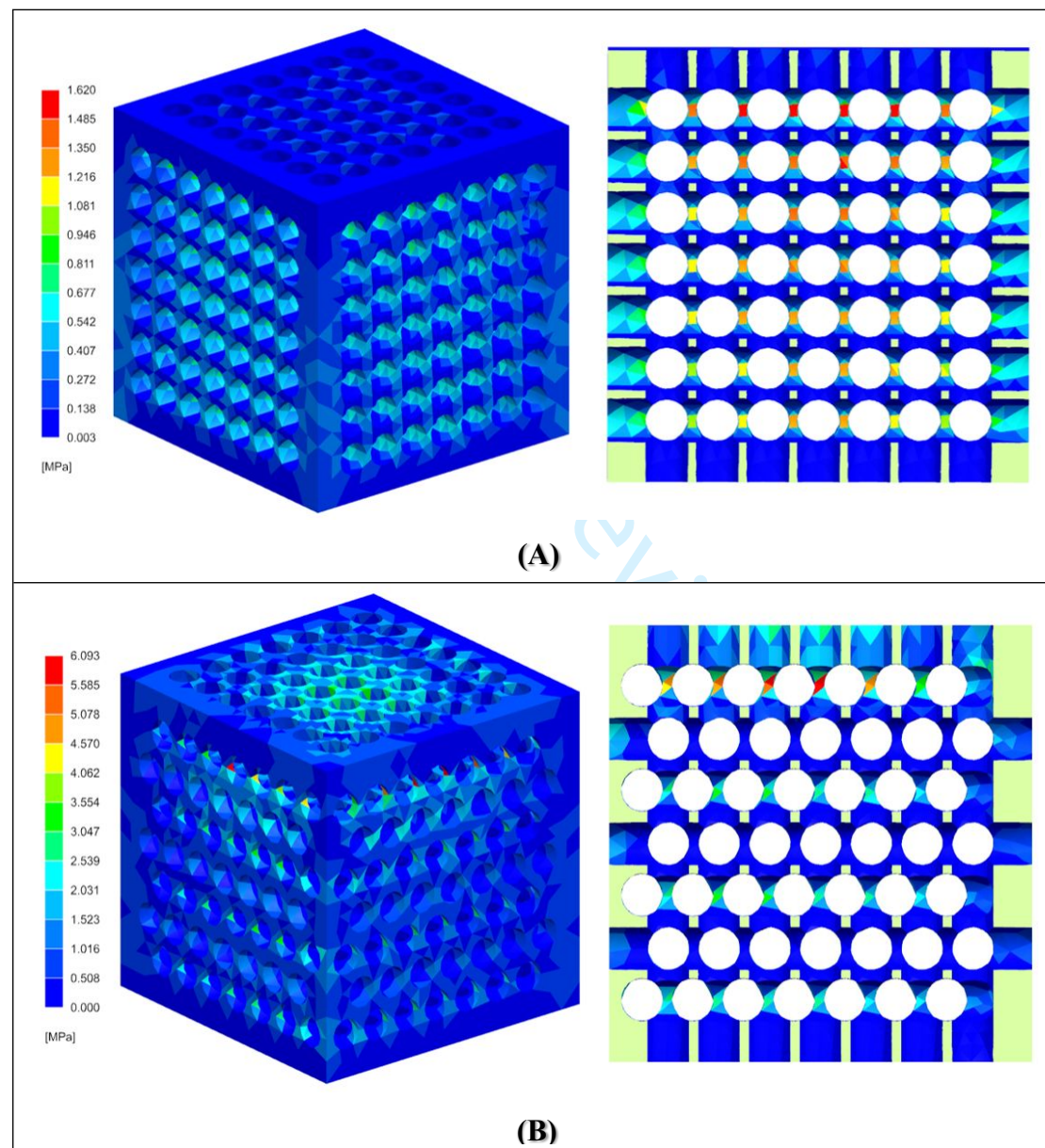
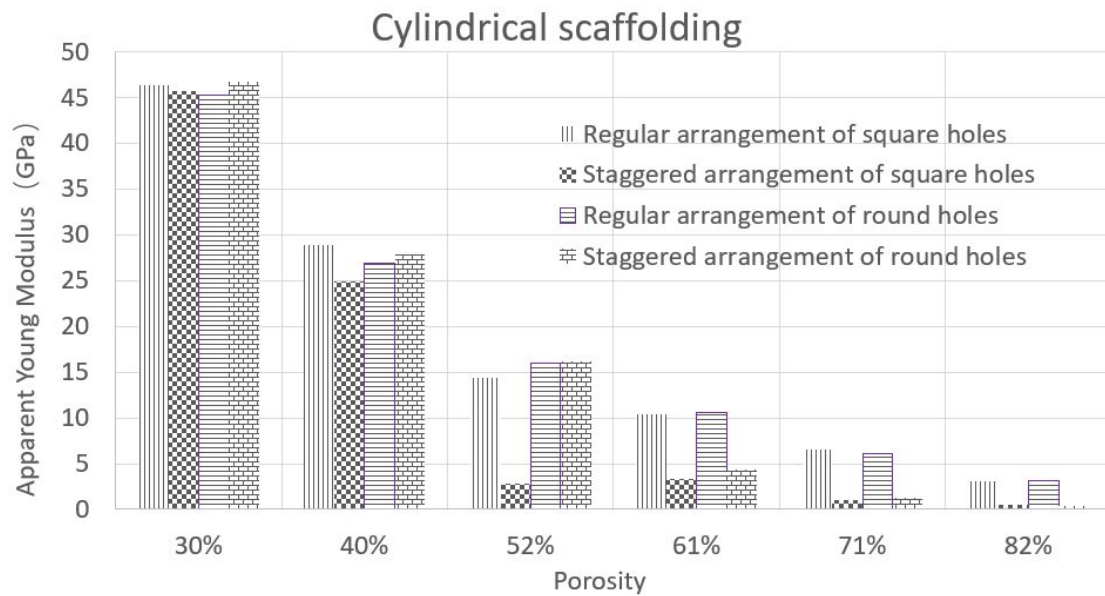


Figure 8: von Mises stress distribution of cubic scaffolding with round holes

1
2
3
4 The scaffold with round holes Figure 8(A) has a more regular stress distribution, and
5 its stress gradually increases toward the center of the model and the surface where the
6 load is applied. The stress of the staggered round-hole scaffold (Figure 8(B)) is also
7 very concentrated, and it is also distributed on the pillar closest to the loading surface.
8 Still, a small amount of stress distribution can be clearly seen on the loading surface,
9 and its maximum stress distribution is at the center of the circle on the pillar nearby.
10 Among them, the vertical arrangement of square-hole scaffolds in Figure 7 (A) has the
11 smallest maximum stress among the eight designs of scaffolding, which is about 1/93
12 of that of the scaffolds with staggered round holes in Figure 6 (B). The design with the
13 most massive stress among the cubic scaffolds is the cubic scaffold with staggered
14 round holes. According to Figures 7 and 8, it can be seen that when the holes are
15 arranged in the same way, the scaffold with square holes is less likely to have stress
16 concentration than the round hole scaffold, and its stress distribution is more uniform.
17 Especially in Figure 7(A), the stress is more evenly dispersed inside the scaffold. Such
18 scaffolding has better mechanical performance, and the structure is not easily damaged.
19
20
21
22
23
24
25
26
27
28
29
30
31
32
33
34

35 Combined with the above results, it is shown that the staggered arrangement of holes is
36 more likely to cause the stress concentration of the scaffold than the scaffold with a
37 more regular vertical arrangement of holes. The stress of the cylindrical element
38 scaffold in this arrangement is mainly concentrated on the surface where the load is
39 applied, while the stress of the cubic element scaffold is mainly concentrated on the
40 pillar closest to the surface although it is distributed inside the model. Regardless of
41 whether the scaffolds have round holes or square holes, their maximum stress is always
42 higher than that of scaffolds arranged vertically due to the more concentrated stress.
43 And the maximum stress of the round hole cylindrical scaffold (Figure 6 (D)) is the
44 largest among these eight models. The shape of the hole will also affect the stent. The
45 loading capacity of a round hole is not as good as that of a square hole, and the
46 maximum stress is concentrated near the loading surface, which is more likely to cause
47 stress concentration.
48
49
50
51
52
53
54
55
56
57
58
59
60



24 Figure 9: The relationship between the porosity and apparent Young's modulus of
25 cylindrical scaffold
26

27
28
29
30 Figures 9 and 10 show the variation of the apparent Young's modulus of the scaffold
31 with porosity. The results show that for these eight models, the apparent Young's
32 modulus decreases as the porosity changes due to the evolution of pore size, and there
33 is a linear behaviour between the porosity and the apparent Young's modulus. It can be
34 seen from Figure 9 that for the cylindrical scaffold, whether the shape of the hole is
35 round or square, the apparent Young's modulus of the two regular porous scaffolds is
36 almost the same under the same porosity. The staggered perforated scaffolding shows
37 different behaviours. When the porosity of the staggered round-hole scaffold is less
38 than or equal to 50%, its apparent Young's modulus is higher than that of the regularly
39 arranged scaffold. This behaviour may be since when the porosity is low, the internal
40 structure of the scaffold is more solid due to the staggered offset. When the porosity is
41 higher than 50%, its apparent Young's modulus is reduced to less than that of scaffolds
42 with regular holes. Regardless of the porosity of the staggered square-hole scaffold, its
43 apparent Young's modulus is smaller than the other three models. And its reduction is
44 relatively significant, with a slight rebound between 50% and 60%, but it is still a
45 downward trend in the end. It can be seen in Figure 9 that the apparent Young's
46
47
48
49
50
51
52
53
54
55
56
57
58
59
60

modulus of the two staggered porous scaffolds is different under low porosity. As the apparent Young's modulus increases, their apparent Young's modulus gradually tends to be consistent. For cylindrical scaffolding, the shape of the hole has little effect on the mechanical properties. Especially after the porosity is higher than 60%, the apparent Young's modulus of scaffolds with the same hole arrangement and different hole types are the same.

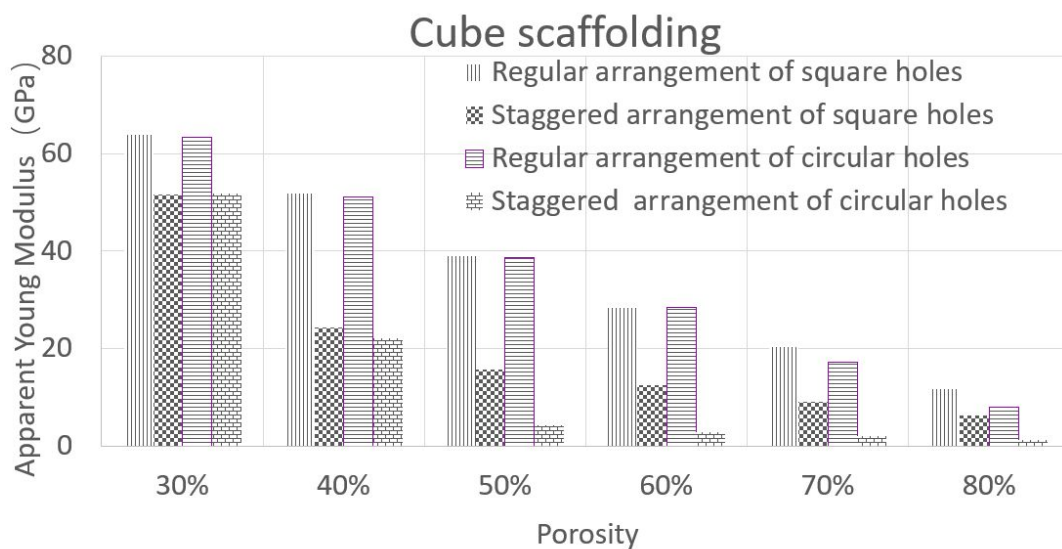


Figure 10: Relationship between the porosity and apparent Young's modulus of cube scaffolding

When the basic shape of the scaffold is a cube (Figure 10), no matter the way of the holes is square or round, the apparent Young's modulus of the scaffold with the staggered porous arrangement is smaller than that of the regularly arranged holes at any porosity. For the scaffold with the regular porous arrangement, when the porosity is less than or equal to 60%, the apparent Young's modulus of the two is almost the same at any porosity. With the increase of porosity, the apparent Young's modulus of the scaffold with square holes under high porosity is more significant than that with round holes. However, the two staggered porous scaffolds exhibit similar behaviour at a low porosity of 30%. When the porosity is higher than 40%, as the porosity increases, the apparent Young's modulus of the round-pored scaffold decreases rapidly, and the apparent Young's modulus of the scaffold has been smaller than the

1
2
3
4 square hole. Cube scaffolding is different from a cylinder, and the shape of the hole
5 does not affect the scaffold with low porosity. When the porosity is high, the apparent
6 Young's modulus of different hole types is slightly different.
7
8
9

10
11 The results show that with the increase of porosity, the apparent Young's modulus of
12 tissue engineering scaffold gradually decreases. The decrease in mechanical properties
13 caused by high porosity will damage the scaffold prematurely, which will limit the
14 choice of tissue scaffold porosity [31]. Regardless of the scaffold design, under the
15 same porosity, the apparent Young's modulus of the scaffolds with two different hole
16 arrangement designs is quite different, and the tissue engineering scaffold with the holes
17 arranged vertically has a better apparent Young's modulus. The mechanical properties
18 of scaffolding are not only affected by porosity, but also by the arrangement of holes.
19
20
21
22
23
24
25
26
27
28

29 The apparent Young's modulus of human cortical bone has an extensive elastic range
30 due to the difference in the location of the bone test and the test conditions, and its
31 apparent Young's modulus is between 7.4 and 31.6 GPa [32]. Tissue scaffolding with
32 high porosity can promote the growth and value-added of cells in the body [33].
33 Scaffolding, as a substitute for damaged tissues or organs, must satisfy the combination
34 of biocompatibility and mechanical properties. Therefore, the main concern here is the
35 mechanical properties of scaffolds with porosity higher than 50%. The regular porous
36 cylindrical scaffold satisfies the apparent Young's modulus range of human cortical
37 bone at a porosity of 50% to 60%, and the apparent Young's modulus of round holes is
38 slightly higher than that of square holes. It is worth noting that the staggered round-
39 hole scaffold also meets the requirements under this porosity. For cubic scaffolds, the
40 apparent Young's modulus of the two regularly arranged scaffolds meets the conditions
41 when the porosity is higher than 60% and less than 80%, and their apparent Young's
42 modulus is larger than that of the cylindrical scaffold with the same porosity. Although
43 the apparent Young's modulus of the staggered square-hole cubic scaffold is not as
44 good as that of the regular arrangement, it also conforms to the apparent Young's
45 modulus range of cortical bone within the porosity range of 50% to 80%. Comparing
46
47
48
49
50
51
52
53
54
55
56
57
58
59
60

1
2
3
4 the above scaffolding, it can be found that the regularly arranged square-hole cubic
5 scaffolding performs best in all scaffolding designs, that is, it has excellent mechanical
6 properties under high porosity.
7
8
9

10 11 **4. Conclusions** 12

13
14 This study designs eight tissue engineering scaffolds with cubes and cylinders as
15 essential elements, utilizing round and square holes to investigate the effect of pore
16 distribution on mechanical properties through finite element analysis. The research
17 concludes that cylindrical scaffolds with circular holes have a slightly higher apparent
18 Young's modulus within the 30%-50% porosity range. Scaffolds with vertically
19 arranged holes exhibit better loading capacity but are more prone to stress concentration.
20 The apparent Young's modulus of cube-based designs is higher than that of cylinder-
21 based designs at any porosity, and the shape of the hole has little effect on the
22 mechanical properties of the scaffold. The cubic scaffold with a regular porous
23 arrangement performs the best in mimicking the mechanical properties of human
24 cortical bone. Misaligned holes decrease the mechanical properties of scaffolds with
25 the same porosity.
26
27
28
29
30
31
32
33
34
35
36
37
38
39
40
41
42
43
44
45
46
47
48
49
50
51
52
53
54
55
56
57

58 **Reference** 59 60

1
2
3
4 [1]. Kenkre JS, Bassett JH. The bone remodelling cycle. *Annals of clinical*
5 *biochemistry*. 2018 May;55(3):308-27.

6
7 [2]. Hollister SJ. Porous scaffold design for tissue engineering. *Nature*
8 *materials*. 2005 Jul 1;4(7):518-24.

9
10 [3]. O'brien FJ. Biomaterials & scaffolds for tissue engineering. *Materials*
11 *today*. 2011 Mar 1;14(3):88-95.

12
13 [4]. Niinomi M, Nakai M, Hieda J. Development of new metallic alloys for
14 *biomedical applications*. *Acta biomaterialia*. 2012 Nov 1;8(11):3888-903.

15
16 [5]. Malladi L, Mahapatro A, Gomes AS. Fabrication of magnesium-based
17 *metallic scaffolds for bone tissue engineering*. *Materials technology*. 2018 Jan
18 28;33(2):173-82.

19
20 [6]. Roy S, Panda D, Khutia N, Chowdhury AR. Pore geometry optimization
21 *of titanium (Ti6Al4V) alloy, for its application in the fabrication of customized hip*
22 *implants*. *International Journal of Biomaterials*. 2014 Oct 21;2014.

23
24 [7]. Van Noort R. Titanium: the implant material of today. *Journal of Materials*
25 *Science*. 1987 Nov; 22:3801-11.

26
27 [8] Yu G, Li Z, Li S, Zhang Q, Hua Y, Liu H, Zhao X, Dhaidhai DT, Li W,
28 Wang X. The select of internal architecture for porous Ti alloy scaffold: A
29 *compromise between mechanical properties and permeability*. *Materials & Design*.
30 2020 Jul 1;192:108754.

31
32 [9]. Long M, Rack HJ. Titanium alloys in total joint replacement—a materials
33 *science perspective*. *Biomaterials*. 1998 Sep 1;19(18):1621-39.

34
35 [10]. Xue W, Krishna BV, Bandyopadhyay A, Bose S. Processing and
36 *biocompatibility evaluation of laser processed porous titanium*. *Acta biomaterialia*.
37 2007 Nov 1;3(6):1007-18.

38
39 [11]. Li Y, Yang C, Zhao H, Qu S, Li X, Li Y. New developments of Ti-based
40 *alloys for biomedical applications*. *Materials*. 2014 Mar 4;7(3):1709-800.

41
42 [12]. Sun W, Darling A, Starly B, Nam J. Computer-aided tissue engineering:
43 *overview, scope and challenges*. *Biotechnology and applied biochemistry*. 2004
44 Feb;39(1):29-47.

1
2
3
4 [13]. Cansizoglu O, Harrysson OL, Cormier D, West H, Mahale T. Properties
5 of Ti-6Al-4V non-stochastic lattice structures fabricated via electron beam melting.
6 Materials Science and Engineering: A. 2008 Sep 25;492(1-2):468-74.
7

8
9 [14]. Kadkhodapour J, Montazerian H, Raeisi S. Investigating internal
10 architecture effect in plastic deformation and failure for TPMS-based scaffolds
11 using simulation methods and experimental procedure. Materials Science and
12 Engineering: C. 2014 Oct 1;43:587-97.
13
14

15
16 [15]. Giannitelli SM, Accoto D, Trombetta M, Rainer A. Current trends in the
17 design of scaffolds for computer-aided tissue engineering. Acta biomaterialia. 2014
18 Feb 1;10(2):580-94.
19
20

21
22 [16]. Ali D, Sen S. Finite element analysis of mechanical behavior,
23 permeability and fluid induced wall shear stress of high porosity scaffolds with
24 gyroid and lattice-based architectures. Journal of the mechanical behavior of
25 biomedical materials. 2017 Nov 1;75:262-70.
26
27
28

29
30 [17]. Filardi V. Stress shielding analysis on easy step staple prosthesis for
31 calcaneus fractures. Journal of Orthopaedics. 2020 Mar 1;18:132-7.
32
33

34
35 [18] Niinomi M, Nakai M. Titanium-based biomaterials for preventing stress
36 shielding between implant devices and bone. International journal of biomaterials.
37 2011 Jan 1;2011.
38
39

40
41 [19]. Ambu R, Morabito AE. Porous scaffold design based on minimal
42 surfaces: Development and assessment of variable architectures. Symmetry. 2018
43 Aug 25;10(9):361.
44
45

46
47 [20]. Zhang XY, Fang G, Xing LL, Liu W, Zhou J. Effect of porosity variation
48 strategy on the performance of functionally graded Ti-6Al-4V scaffolds for bone
49 tissue engineering. Materials & Design. 2018 Nov 5;157:523-38.
50
51

52
53 [21]. Van Grunsven W, Hernandez-Nava E, Reilly GC, Goodall R. Fabrication
54 and mechanical characterisation of titanium lattices with graded porosity. Metals.
55 2014 Aug 14;4(3):401-9
56
57

58
59 [22]. Zhou H, Zhao M, Ma Z, Zhang DZ, Fu G. Sheet and network based
60 functionally graded lattice structures manufactured by selective laser melting:

1
2
3
4 Design, mechanical properties, and simulation. *International Journal of Mechanical*
5 *Sciences*. 2020 Jun 1; 175:105480

6
7 [23]. Nune KC, Kumar A, Misra RD, Li SJ, Hao YL, Yang R. Functional
8 response of osteoblasts in functionally gradient titanium alloy mesh arrays
9 processed by 3D additive manufacturing. *Colloids and Surfaces B: Biointerfaces*.
10 2017 Feb 1; 150:78-88.

11
12 [24]. Wieding J, Jonitz A, Bader R. The effect of structural design on
13 mechanical properties and cellular response of additive manufactured titanium
14 scaffolds. *Materials*. 2012 Aug 10;5(8):1336-47

15
16 [25]. Pattanayak DK, Fukuda A, Matsushita T, Takemoto M, Fujibayashi S,
17 Sasaki K, Nishida N, Nakamura T, Kokubo T. Bioactive Ti metal analogous to
18 human cancellous bone: Fabrication by selective laser melting and chemical
19 treatments. *Acta Biomaterialia*. 2011 Mar 1;7(3):1398-406

20
21 [26]. Wu S, Liu X, Yeung KW, Liu C, Yang X. Biomimetic porous scaffolds
22 for bone tissue engineering. *Materials Science and Engineering: R: Reports*. 2014
23 Jun 1;80:1-36.

24
25 [27]. Li S, Zhao S, Hou W, Teng C, Hao Y, Li Y, Yang R, Misra RD.
26 Functionally graded Ti-6Al-4V meshes with high strength and energy absorption.
27 *Advanced Engineering Materials*. 2016 Jan;18(1):34-8.

28
29 [28] Jin H, Zhuo Y, Sun Y, Fu H, Han Z. Microstructure design and
30 degradation performance in vitro of three-dimensional printed bioscaffold for bone
31 tissue engineering. *Advances in Mechanical Engineering*. 2019
32 Oct;11(10):1687814019883784.

33
34 [29] Shi C, Lu N, Qin Y, Liu M, Li H, Li H. Study on mechanical properties
35 and permeability of elliptical porous scaffold based on the SLM manufactured
36 medical Ti6Al4V. *PLoS One*. 2021 Mar 4;16(3):e0247764.

37
38 [30] Szymczyk P, Hoppe V, Ziółkowski G, Smolnicki M, Madeja M. The
39 effect of geometry on mechanical properties of Ti6Al4V ELI scaffolds
40 manufactured using additive manufacturing technology. *Archives of Civil and*
41 *Mechanical Engineering*. 2020 Mar;20:1-3.
42
43
44
45
46
47
48
49
50
51
52
53
54
55
56
57
58
59
60

1
2
3
4 [31]. Karageorgiou V, Kaplan D. Porosity of 3D biomaterial scaffolds and
5 osteogenesis. *Biomaterials*. 2005 Sep 1;26(27):5474-91.
6

7 [32]. Boughton OR, Ma S, Zhao S, Arnold M, Lewis A, Hansen U, Cobb JP,
8 Giuliani F, Abel RL. Measuring bone stiffness using spherical indentation. *PLoS*
9 *One*. 2018 Jul 12;13(7):e0200475.
10
11
12

13 [33]. Gomes ME, Holtorf HL, Reis RL, Mikos AG. Influence of the porosity
14 of starch-based fiber mesh scaffolds on the proliferation and osteogenic
15 differentiation of bone marrow stromal cells cultured in a flow perfusion bioreactor.
16 *Tissue engineering*. 2006 Apr 1;12(4):801-9.
17
18
19
20
21
22
23
24
25
26
27
28
29
30
31
32
33
34
35
36
37
38
39
40
41
42
43
44
45
46
47
48
49
50
51
52
53
54
55
56
57
58
59
60